# Spin delocalization of interstitial iron in silicon

van Wezep, D.A.; Gregorkiewicz, T.; Sieverts, E.G.; Ammerlaan, C.A.J.

DOI
10.1103/PhysRevB.34.4511
Publication date
1986

Published in
Physical Review. B, Condensed Matter

# Spin delocalization of interstitial iron in silicon

D. A. van Wezep, T. Gregorkiewicz,* E. G. Sieverts, and C. A. J. Ammerlaan
*Natuurkundig Laboratorium der Universiteit van Amsterdam, Valckenierstraat 65, 1018 XE Amsterdam, The Netherlands*
(Received 7 March 1986)

The apparent contradiction between a covalently delocalized picture of the Si:$Fe_i^0$ system, suggested among others by the large reduction of the central nucleus hyperfine interaction parameter as compared to the free ion, and the localized picture as has emerged from the analysis of a recent electron-nuclear double resonance (ENDOR) experiment, is resolved by a reinterpretation of the ENDOR data in a linear-combination-of-atomic-orbital treatment, that takes the spin multiplicity and symmetry properties of the paramagnetic $(e)^2$ state into account. This reinterpretation is confirmed by the determination of the relative signs of the $^{29}$Si hyperfine interaction tensors in an ENDOR experiment under uniaxial stress. The data obtained are consistent with a 25% spin localization on the first six shells of silicon neighbors.

## I. INTRODUCTION

Recently electron-nuclear double resonance (ENDOR) data on interstitial iron ($Fe_i^0, 3d^8, S=1$) and titanium ($Ti_i^+, 3d^3, S=\frac{3}{2}$) in silicon have become available.[1,2] In the past ENDOR measurements have provided valuable information regarding the distribution of the spin density over the silicon lattice in a variety of systems,[3-7] and, in the case of the shallow donors, these data formed a critical test for the effective-mass theory.[8,9] It may be expected that the $Fe_i^0$ and $Ti_i^+$ ENDOR data provide a stringent test for theoretical calculations on transition metals in silicon as well. The most successful calculations thus far are those by Katayama-Yoshida and Zunger[10,11] and Beeler *et al.*,[12] who reproduce the experimentally observed donor and acceptor levels of the interstitial $3d$ transition metals in the band gap of silicon quite accurately. These self-consistent Green's-function calculations furthermore confirm the phenomenological model of Ludwig and Woodbury,[13] describing the EPR spectra of interstitial and substitutional $3d$ transition metals in silicon for all experimental EPR spectra observed thus far. They also give definite predictions for the spin transfer from the central ion to the silicon lattice: Beeler *et al.* predict a 12% spin transfer for $Fe_i^0$ and a 58% spin transfer for $Ti_i^+$; Katayama-Yoshida and Zunger give a 29% spin delocalization for the $Fe_i^0$ system.

Among the experimental data that can give information about this spin transfer is the observed reduction of the hyperfine interaction parameter $A$ of a transition-metal ion when embedded in a silicon matrix. If the Ludwig-Woodbury model is adopted, this reduction must be due to a reduction in the polarization of the $1s$, $2s$, and $3s$ core states. This polarization is known to be directly proportional to the spin density in the $3d$ orbitals throughout the $3d$ transition series[14] and the observed reductions in $A$ therefore reflect the transfer of spin density to the lattice. The experimental values (for $Fe_i^0$, a 43% reduction[10,13] and for $Ti_i^+$, a 75% reduction[2,15]) thus seem to indicate a substantial spin transfer. Further information can be obtained from an analysis of the parameters describing the interaction of the electronic spin density with the 4.7% abundant magnetic $^{29}$Si nuclei, obtained from EPR (Ref. 16) and ENDOR (Refs. 1 and 2) measurements. The ENDOR measurements on the $Fe_i^0$ system were performed by Greulich-Weber *et al.*, who could assign the

TABLE I. Parameters and orientations of hyperfine tensors of $^{29}$Si neighbors of Si:$Fe_i^0$ (in kHz). Experimental uncertainty is ±10 kHz [from Greulich-Weber *et al.* (Ref. 1)]. For comparison we included the calculated values $b_{dd}$ in the point-dipole approximation, assuming 100% spin localization on the central nucleus and a positive $g$ value.

| Tensor | $a'$ | $b'$ | $c'$ | $Z_{hf}$ | $b_{dd}$ | Shell |
|---|---|---|---|---|---|---|
| *31* | −160 | −1400 | 0 | [111] | −1249.2 | 1 |
| *32* | 780 | −200 | 0 | [111] | −156.2 | 4 or 5 |
| *33* | 3250 | −160 | 0 | [111] | −156.2 | 5 or 4 |
| *T*1 | −4640 | −800 | −520 | [100] | −811.4 | 2 |
| *M*1 | −3870 | −440 | +70 | $<$[111]=11° | −177.9 | 3 |
| *M*2 | −380 | −90 | −2 | $<$[111]=2.6° | −78.4 | 6 |

 

hyperfine interaction tensors to specific shells of silicon neighbors due to a striking correspondence between experimental values of the anisotropic part of these tensors and those calculated in a point-dipole approximation, assuming 95% of the spin density to reside on the iron nucleus. For convenience these results are reproduced in Table I. This interpretation is therefore consistent with a high degree of spin localization on the central nucleus and contradicts the conclusion reached above. In the case of the $Ti_i^+$ data such a correspondence between measured and calculated anisotropic hyperfine interaction parameters could not be found, indicating a larger covalency. In a linear-combination-of-atomic-orbital (LCAO) treatment (reviewed by Owen and Thornley[17]) that takes spin multiplicity and symmetry properties of the paramagnetic ground state into account, an estimate for the minimum spin transfer of the $Ti_i^+$ system ($\sim$40%) could be obtained. In this case the agreement between the experiment (spin transfer between 40% and 75%) and theory (Beeler *et al.*: 58%) is excellent. For $Fe_i^0$ the spin transfer derived from the ENDOR data ($\sim$5%) is reasonably consistent with the calculations by Beeler *et al.*, but it seems that the 12% spin transfer they obtain cannot be held solely responsible for the above-mentioned 43% reduction in $A$. In contrast, Katayama-Yoshida and Zunger obtain reasonable agreement between the calculated and experimental hyperfine field on the Fe nucleus, but find a 29% spin delocalization at variance with the ENDOR results. The basic problem is, of course, the contradiction between the spin transfer as derived from $^{29}$Si ENDOR ($\sim$5%), and that obtained from the reduction in $A$ for $^{57}$Fe ($\sim$43%). It will be shown in the following that this difficulty can be resolved by applying the same LCAO treatment as used for the analysis of the $Ti_i^+$ ENDOR data, instead of the one-electron treatment of Watkins and Corbett[18] that was applied in the description of $S=\frac{1}{2}$ systems and was also used in Ref. 1. It allows an interpretation of the Fe ENDOR data in which the spin density is more delocalized than the 5% obtained by Greulich-Weber *et al.*, even when corrections for the distant dipole-dipole interaction are taken into account. We will furthermore present evidence supporting this interpretation, obtained from an ENDOR experiment on the Si:$Fe_i^0$ system with simultaneous application of uniaxial compressive stress. This allowed the experimental determination of the relative signs of the hyperfine interaction tensors and the elimination of the existing ambiguity in interpretation of the ENDOR data.

## II. PRELIMINARIES

### A. Symmetry orbitals and hyperfine interaction tensors

The LCAO treatment that will apply to the $Fe_i^0$ case is entirely equivalent to the case of $Ti_i^+$; approximations and calculational procedures have already been discussed in detail in Ref. 2, to which we also refer for notation. The systems are different, however, in their ground states; paramagnetism arises from three electrons in $t_2$ states for $Ti_i^+$ and from two electrons in $e$ states for $Fe_i^0$. Consequently, we will describe the wave function of the $Fe_i^0$

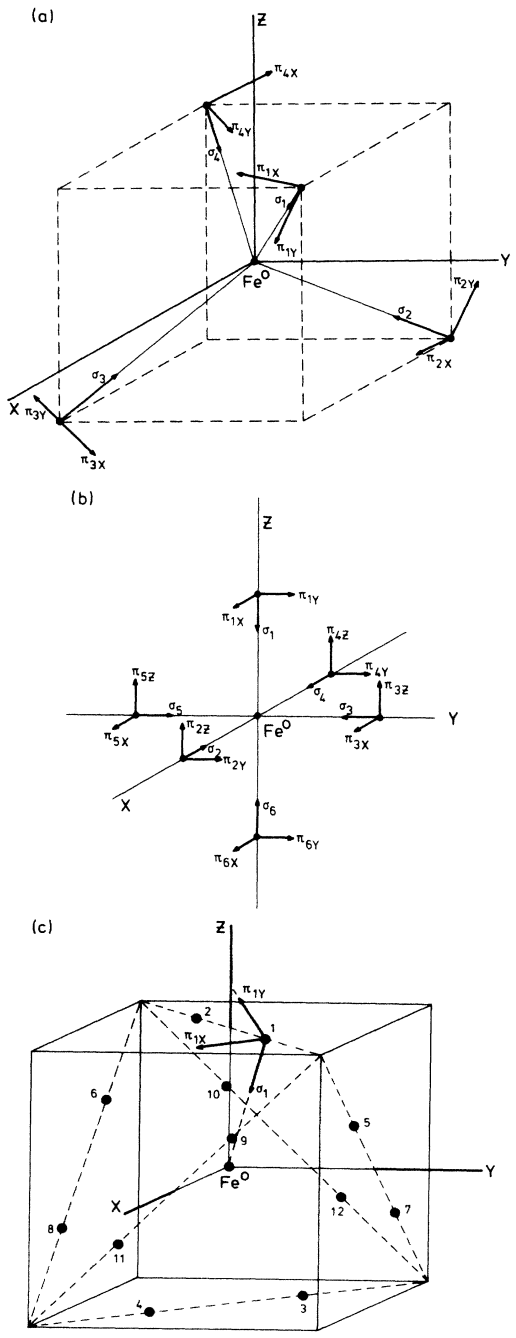


FIG. 1. Orientations of $\sigma$ and $\pi$ orbitals on atoms of the different symmetry shells. The $\sigma$ orbitals are always taken to point into the direction of the central ion for all shells. (a) A 3-class shell. The numbers 1, 2, 3, and 4 refer to the ligands at positions $nnn$, $\bar{n}n\bar{n}$, $n\bar{n}\bar{n}$, and $\bar{n}\bar{n}n$ ($n$ integer), respectively. The $\pi_{1x}$ and $\pi_{1y}$ orbitals are along $[1\bar{2}1]$ and $[10\bar{1}]$ directions, respectively. Orientations of the orbitals on 2, 3, and 4 are obtained by $C_2$ rotations about the $x$, $y$, and $z$ axes. (b) A $2mm$-class shell. The numbers 1 to 6 refer to positions $002n$, $2n00$, $02n0$, $2\bar{n}00$, $02\bar{n}0$, $00 2\bar{n}$. The $\pi$ orbitals are along the positive $x$, $y$, and $z$ directions for all atoms. (c) A $m$-class shell. The numbers 1 to 12 refer to $nnm$, $\bar{n}\bar{n}m$, $\bar{n}n\bar{m}$, $n\bar{n}\bar{m}$, $nmn$, $\bar{n}m\bar{n}$, $\bar{n}m\bar{n}$, $n\bar{m}\bar{n}$, $mnn$, $\bar{m}\bar{n}n$, $m\bar{n}\bar{n}$, and $\bar{m}n\bar{n}$. The $\pi_{1x}$ and $\pi_{1y}$ orbitals are along $[1\bar{1}0]$ and $[\bar{m}\,\bar{m}\,2n]$, respectively. Orientations of the orbitals on 2 to 12 are obtained by $C_2$ and $C_3$ rotations of the silicon lattice.

ground state by taking linear combinations of $3s$ and $3p$ orbitals of the silicon lattice which transform as the $e$ irreducible representation of the $\bar{4}3m$ symmetry point group and admix these to the $d_{x^2-y^2}$ and $d_{3z^2-r^2}$ orbitals of the same $e$ representation.

For a 3-class shell, with atom positions and ligand orbitals as shown in Fig. 1(a), we obtain the following expressions for the symmetry orbitals:

$$\Psi_{3z^2-r^2}=\alpha d_{3z^2-r^2}+\tfrac{1}{4}\delta_i[(\pi_{1x}+\pi_{2x}+\pi_{3x}+\pi_{4x}) -\sqrt{3}(\pi_{1y}+\pi_{2y}+\pi_{3y}+\pi_{4y})],$$
$$\Psi_{x^2-y^2}=\alpha d_{x^2-y^2}+\tfrac{1}{4}\delta_i[(\pi_{1y}+\pi_{2y}+\pi_{3y}+\pi_{4y}) +\sqrt{3}(\pi_{1x}+\pi_{2x}+\pi_{3x}+\pi_{4x})], \tag{1}$$

yielding the following hyperfine interaction tensor for atom 1:

$$\overleftrightarrow{B}=\frac{1}{2S}(\tfrac{1}{4}\delta_i^2)\begin{bmatrix} b & 0 & 0 \\ 0 & b & 0 \\ 0 & 0 & -2b \end{bmatrix} +\frac{1}{2S}(2\alpha^2)\begin{bmatrix} -b_{dd} & 0 & 0 \\ 0 & -b_{dd} & 0 \\ 0 & 0 & 2b_{dd} \end{bmatrix} \tag{2}$$

with $b=\frac{2}{5}(\mu_0/4\pi)g\mu_B g_N\mu_N\langle r^{-3}\rangle_p$ and $b_{dd}=(\mu_0/4\pi)g\mu_B g_N\mu_N R^{-3}$ ($R$ is the Fe-$^{29}$Si distance). The isotropic part $a$ of the hyperfine interaction tensor is zero by symmetry in this approximation. Due to our choice of coordinate system this tensor is on principal axes.

For a $2mm$-class shell [Fig. 1(b)] we get:

$$\Psi_{3z^2-r^2}=\alpha d_{3z^2-r^2}+\frac{1}{\sqrt{12}}\beta_i(2s_1+2s_6-s_2-s_3-s_4-s_5) +\frac{1}{\sqrt{12}}\gamma_i(2\sigma_1+2\sigma_6-\sigma_2-\sigma_3-\sigma_4-\sigma_5),$$
$$\Psi_{x^2-y^2}=\alpha d_{x^2-y^2}+\tfrac{1}{2}\beta_i(s_2+s_4-s_3-s_5) +\tfrac{1}{2}\gamma_i(\sigma_2+\sigma_4-\sigma_3-\sigma_5), \tag{3}$$

yielding the following hyperfine interaction tensor for atom 1:

$$\overleftrightarrow{B}=\frac{1}{2S}(\tfrac{1}{3}\gamma_i^2)\begin{bmatrix} -b & 0 & 0 \\ 0 & -b & 0 \\ 0 & 0 & 2b \end{bmatrix} +\frac{1}{2S}(2\alpha^2)\begin{bmatrix} -b_{dd} & 0 & 0 \\ 0 & -b_{dd} & 0 \\ 0 & 0 & 2b_{dd} \end{bmatrix},$$
$$a=\frac{1}{2S}(\tfrac{1}{3}\beta_i^2)\tfrac{2}{3}\mu_0 g\mu_B g_N\mu_N|s_1(0)|^2=\frac{1}{2S}(\tfrac{1}{3}\beta_i^2)a_0. \tag{4}$$

Note that the off-diagonal element is zero to this order although the tensor is in Cartesian coordinates.

For an $m$-class shell [Fig. 1(c)] we obtain the following symmetry orbitals:

$$\begin{aligned}\Psi_{x^2-y^2}=&\alpha d_{x^2-y^2} \\ &+\frac{1}{\sqrt{8}}\beta_i(-s_5-s_6-s_7-s_8+s_9+s_{10}+s_{11}+s_{12})+\frac{1}{\sqrt{8}}\gamma_i(-\sigma_5-\sigma_6-\sigma_7-\sigma_8+\sigma_9+\sigma_{10}+\sigma_{11}+\sigma_{12}) \\ &+\frac{1}{\sqrt{6}}\delta_i[(\pi_{1x}+\pi_{2x}+\pi_{3x}+\pi_{4x})-\tfrac{1}{2}(\pi_{5x}+\pi_{6x}+\pi_{7x}+\pi_{8x}+\pi_{9x}+\pi_{10x}+\pi_{11x}+\pi_{12x})] \\ &+\frac{1}{\sqrt{8}}\epsilon_i(-\pi_{5y}-\pi_{6y}-\pi_{7y}-\pi_{8y}+\pi_{9y}+\pi_{10y}+\pi_{11y}+\pi_{12y}), \\ \Psi_{3z^2-r^2}=&\alpha d_{3z^2-r^2}+\frac{1}{\sqrt{6}}\beta_i[(s_1+s_2+s_3+s_4)-\tfrac{1}{2}(s_5+s_6+s_7+s_8+s_9+s_{10}+s_{11}+s_{12})] \\ &+\frac{1}{\sqrt{6}}\gamma_i[(\sigma_1+\sigma_2+\sigma_3+\sigma_4)-\tfrac{1}{2}(\sigma_5+\sigma_6+\sigma_7+\sigma_8+\sigma_9+\sigma_{10}+\sigma_{11}+\sigma_{12})] \\ &+\frac{1}{\sqrt{8}}\delta_i(\pi_{5x}+\pi_{6x}+\pi_{7x}+\pi_{8x}-\pi_{9x}-\pi_{10x}-\pi_{11x}-\pi_{12x}) \\ &+\frac{1}{\sqrt{6}}\epsilon_i[(\pi_{1y}+\pi_{2y}+\pi_{3y}+\pi_{4y})-\tfrac{1}{2}(\pi_{5y}+\pi_{6y}+\pi_{7y}+\pi_{8y}+\pi_{9y}+\pi_{10y}+\pi_{11y}+\pi_{12y})],\end{aligned} \tag{5}$$

yielding for atom 1 the hyperfine interaction tensor components:

$$B_{xx}=\frac{1}{2S}[\tfrac{1}{6}(2\delta_i^2-\gamma_i^2-\epsilon_i^2)b-2\alpha^2 b_{dd}],\quad B_{yy}=\frac{1}{2S}[\tfrac{1}{6}(2\epsilon_i^2-\delta_i^2-\gamma_i^2)b-2\alpha^2 b_{dd}],\quad B_{zz}=\frac{1}{2S}[\tfrac{1}{6}(2\gamma_i^2-\delta_i^2-\epsilon_i^2)b+4\alpha^2 b_{dd}],$$
$$B_{yz}=B_{zy}=\frac{1}{2S}\frac{1}{2}\gamma_i\epsilon_i b,\quad B_{xy}=B_{yx}=B_{xz}=B_{zx}=0,$$
$$a=\frac{1}{2S}(\tfrac{1}{6}\beta_i^2)a_0. \tag{6}$$

This tensor is given in the $\sigma\pi_x\pi_y$ coordinate system defined in Fig. 1(c).

As Greulich-Weber *et al.* did not observe any hyperfine interaction with lattice sites of general symmetry this type of shell is not considered.

The transfer to the $\pi$ orbitals for $2mm$ shells turns out to be forbidden; as a consequence the Cartesian hyperfine tensor contains to first order no off-diagonal terms and is exactly $\langle 100 \rangle$ axial. Experimentally these tensors were found to have their largest eigenvector along the $\langle 100 \rangle$ axis, but are not really axial as evidenced by the $b'/c'$ ratio of about 1.5. Still we can conclude that the distant dipole-dipole interaction with the spin density on the central ion and transfer to the $\sigma$ orbital dominate the hyperfine interaction, especially when compared to the $Ti_i^+$ system, where the transfer to the $\pi$ orbitals is allowed and dominant, resulting in an approximate $\langle 011 \rangle$ axiality of these tensors. For this latter system the off-diagonal tensor element is 4751.6 kHz,[2] which is an order of magnitude larger than for $Fe_i^0$, where it amounts to 520 kHz.[1] The magnitude of the off-diagonal tensor element could possibly be explained by including the multicenter contributions in the calculation of Eq. (4); for the moment this first-order approximation will suffice however.

In the case of the *3*-class shells the transfer to $s$ and $\sigma$ orbitals is forbidden. The spin density in the $\pi$ orbitals gives rise to a contribution to $\vec{B}$ opposite in sign to that of the distant dipole-dipole interaction and therefore opposite in sign to (and moreover half the size of) that found in the more usual one-electron treatment.[18] The sign of $b'$ is thus dependent on which of these contributions dominates the hyperfine interaction, which could be determined experimentally if $a'$ was determined by spin transfer and not required to be zero. Experimentally $a'$ values are found to be nonzero and in one instance (tensor *33*) of substantial magnitude (although the corresponding spin density would be less than 0.3%). It could be that $a'$ for *3*-class shells is determined by exchange polarization of the closed electron shells on the ligands as proposed in Ref. 1, an effect we did not consider in deriving Eq. (2). This (and the fact that the off-diagonal element of $T1$ is nonzero) might be taken as evidence that the paramagnetism does not arise from the $e$ states only and would confirm a result from the spin-polarized Green's-function calculations by Katayama-Yoshida and Zunger[10] where a 5:1 magnetic moment distribution over the $e$ and $t_2$ states is obtained as a result of the polarization of the filled $t_2$ states by the spin density in the $e$ states. The unbalance in the spin up-down transfer from the $t_2$ states to the lattice could give rise to additional hyperfine interaction. The isotropic part $a'$ of the *3*-class shells is then not necessarily of the same sign as for the other symmetry shells, where spin transfer from the $e$ state is allowed and can be expected to dominate all other effects. This has been recognized by Greulich-Weber *et al.*, who take the opposite sign of $a'$ for tensors *32* and *33* (in comparison to the other four) in order to arrive at the correspondence between $b_{\text{expt}}$ and $b_{dd}$. Since the overall sign of the hyperfine interaction tensors cannot be inferred from the ENDOR data, this is a legitimate choice and a reasonable one, in view of the correspondence above. If one assumes however that this agreement is only fortuitous and takes the sign of $a'$ for tensor *31* equal to that of tensors *32* and *33*, the estimate of the spin density on the first-neighbor shell increases from a mere 1% to some 15%, since the sign of $b'$ must be reversed simultaneously. It is obvious that this latter interpretation is in far better agreement with the observed reduction in central nucleus hyperfine constant than that by Greulich-Weber *et al.* Another argument in favor could be the fact that (for 90% spin localization on the central ion and the experimental sign as chosen in Ref. 1)

$$b'-b_{dd}=1400\text{ kHz}-0.9(1250\text{ kHz})=275\text{ kHz}$$

of the hyperfine interaction must be due to a spin density in the *forbidden* $\sigma$ orbital, since it is of the same sign as $b_{dd}$. That the transfer to the forbidden $\sigma$ orbital would dominate over the transfer to the allowed $\pi$ orbitals already for the first shell is rather unlikely. On the other hand it may also be argued that the difference is only due to the inaccuracy of the point-dipole approximation and/or the neglect of the multicenter contributions in calculating Eq. (2). At best we may conclude from these considerations that the Fe ENDOR data are not necessarily inconsistent with a delocalized spin density. It is obvious that this is critically dependent on the overall sign of the hyperfine interaction tensors, making an experimental determination of these signs very relevant.

### B. ENDOR under uniaxial stress

Greulich-Weber *et al.* analyzed their data with the following spin Hamiltonian, containing electronic Zeeman, hyperfine, and nuclear Zeeman interaction terms:

$$\mathcal{H}=g\mu_B\mathbf{B}\cdot\mathbf{S}+\sum_i(\mathbf{S}\cdot\vec{A}_i\cdot\mathbf{I}_i-g_N\mu_N\mathbf{B}\cdot\mathbf{I}_i)\,, \tag{7}$$

where the parameter $i$ enumerates the lattice sites around the defect. For an $S=1$, $I=\frac{1}{2}$ system this gives rise to the level scheme of Fig. 2, where the EPR and ENDOR

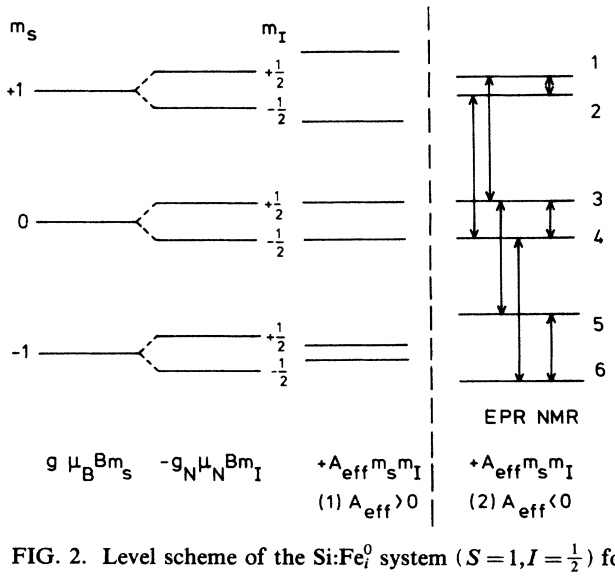


FIG. 2. Level scheme of the Si:$Fe_i^0$ system ($S=1, I=\frac{1}{2}$) for $A_{\text{eff}}>0$ (1) and $A_{\text{eff}}<0$ (2). Level ordering is consistent with $g=+2.070$ and $g_N=-1.1097$, but is not to scale.

transitions are also indicated. The ENDOR transitions are to first order given by:

$$h\nu = \Delta E = |g_N \mu_N B - \hat{\mathbf{h}} \cdot \overleftrightarrow{A} \cdot \hat{\mathbf{h}} m_s| \ , \tag{8}$$

with $\hat{\mathbf{h}}$ a unit vector along the magnetic field **B**. The ENDOR spectrum is thus seen to be symmetric around the nuclear Zeeman frequency $\nu_z = g_N \mu_N B/h$. For a given orientation of the magnetic field and for each Fe-$^{29}$Si orientation in the lattice we therefore expect to find three ENDOR lines, one above, one at, and one below $\nu_z$ (unless the ENDOR pattern is so anisotropic that the Zeeman frequency is crossed as, e.g., happens for tensor *31* where, as a result of second-order effects, there can be two frequencies below or above $\nu_z$ for certain directions of **B**; this does not change the essence of the following, however). Experimentally the ENDOR transitions are obtained by monitoring the EPR intensity while scanning the radio frequency; when an NMR transition is passed, this will result in an intensity change of the EPR signal. Since the ENDOR mechanism is based on spin-relaxation processes, the intensity of an EPR line will be affected more by an NMR transition connected directly to it, than by an NMR transition that is only indirectly coupled. Experimentally this effect has already been observed for $Ti_i^+$ and $Cr_i^+$ in silicon,[19,20] and may be expected to occur for the $Fe_i^0$ system as well. The ENDOR effect of transition $1 \leftrightarrow 2$ for instance is expected to be larger on EPR transitions $1 \leftrightarrow 3/2 \leftrightarrow 4$ than on EPR transitions $3 \leftrightarrow 5/4 \leftrightarrow 6$, while the reverse will be true for NMR transition $5 \leftrightarrow 6$. Depending on the sign of $A_{\text{eff}} = \hat{\mathbf{h}} \cdot \overleftrightarrow{A} \cdot \hat{\mathbf{h}}$ we will either observe the resonance above the Zeeman frequency more strongly on EPR transitions $1 \leftrightarrow 3/2 \leftrightarrow 4$ (situation 1) or that below $\nu_z$ (situation 2), while the reverse holds for EPR transitions $3 \leftrightarrow 5/4 \leftrightarrow 6$. Unfortunately the EPR fine structure vanishes in cubic symmetry and a distinction between situations 1 and 2 cannot be made. It is however possible to separate transitions $1 \leftrightarrow 3/2 \leftrightarrow 4$ from $3 \leftrightarrow 5/4 \leftrightarrow 6$ by applying uniaxial stress,[13,21] which will reveal itself in EPR by a splitting of the $Fe_i^0$ resonance into two components as shown in Fig. 3. Formally this is accounted for by augmenting the spin Hamiltonian Eq. (7) with a term $\mathbf{S} \cdot \overleftrightarrow{D} \cdot \mathbf{S}$, that does not affect the ENDOR frequencies to first order, but separates transitions $1 \leftrightarrow 3/2 \leftrightarrow 4$ considerably from $3 \leftrightarrow 5/4 \leftrightarrow 6$. By performing ENDOR on both stress-split EPR lines separately it becomes possible to distinguish between situations 1 and 2, allowing the determination of the relative signs of the hyperfine interaction tensors. If the sign of the $g$ value is known it is even possible to establish the absolute sign, due to the thermal population difference of the three level-pairs, leading to the intensity difference of the stress-split EPR lines (Fig. 3).

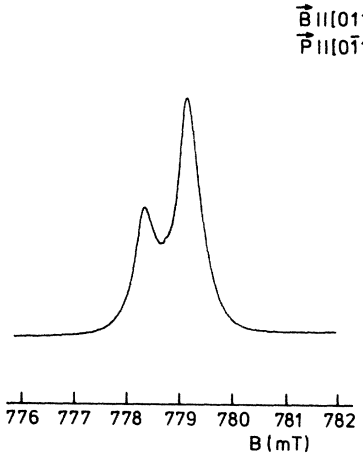


FIG. 3. Recorder trace of the $Fe_i^0$ EPR spectrum at 1.5 K and $\nu_\mu = 22.5682$ GHz, **B**||[011] under [0$\bar{1}$1] uniaxial compressive stress $P = 4.4$ MPa.

## III. EXPERIMENTAL

### A. Procedure

Floating-zone dislocation-free P-doped silicon samples ($15 \times 2 \times 2$ mm$^3$, initial resistivity 100 Ω cm) were scratched with iron and subsequently annealed for 17 h at 1250 °C under argon atmosphere in a closed quartz ampoule. After diffusion the samples were quenched from 1250 °C separately with various quenching speeds, ground and chemically etched in order to remove a layer of approximately 0.1 mm. The samples were then stored at 77 K until the measurements. In all these samples the $Fe_i^0$ EPR spectrum could be observed; the best signal (large signal-to-noise ratio, little line broadening due to internal stresses) was obtained from the sample most rapidly quenched, that was therefore selected for the ENDOR measurements.

These measurements were performed with a superheterodyne spectrometer operating at 23 GHz and adjusted to detect the dispersion part of the EPR signal at an incident microwave power of 1 μW. The magnetic field could be rotated in the (0$\bar{1}$1) plane of the sample and was modulated at a frequency of 83 Hz. In order to separate the EPR transitions we could apply compressive stress along the [0$\bar{1}$1] direction via a stainless-steel rod. We used a silver-coated Epibond cavity; in the thin silver layer on the cylindrical side wall of the cavity a spiral groove was cut, making it suitable as an ENDOR coil.[3] For ENDOR measurements the rf field was square-wave modulated at 3.3 Hz to allow double phase-sensitive detection of the signal. The sample was held at 1.5 K by pumping the He bath.

### B. Results

The ENDOR resonance frequencies were computed with the spin Hamiltonian Eq. (7) and the hyperfine parameters as given by Greulich-Weber *et al.* for the six shells measured. The regions around these frequencies were scanned in ENDOR with the magnetic field along the [100], [111], and [011] directions without applied stress. No resonances of $M1$ and $T1$ could be observed below the Zeeman frequency; although it is possible that our ENDOR coil is less efficient in the low-frequency region where these resonances are expected, it is more likely that our passage conditions were unfavorable for their detection. These resonances are however not really necessary for the sign determination of the tensors. In order to

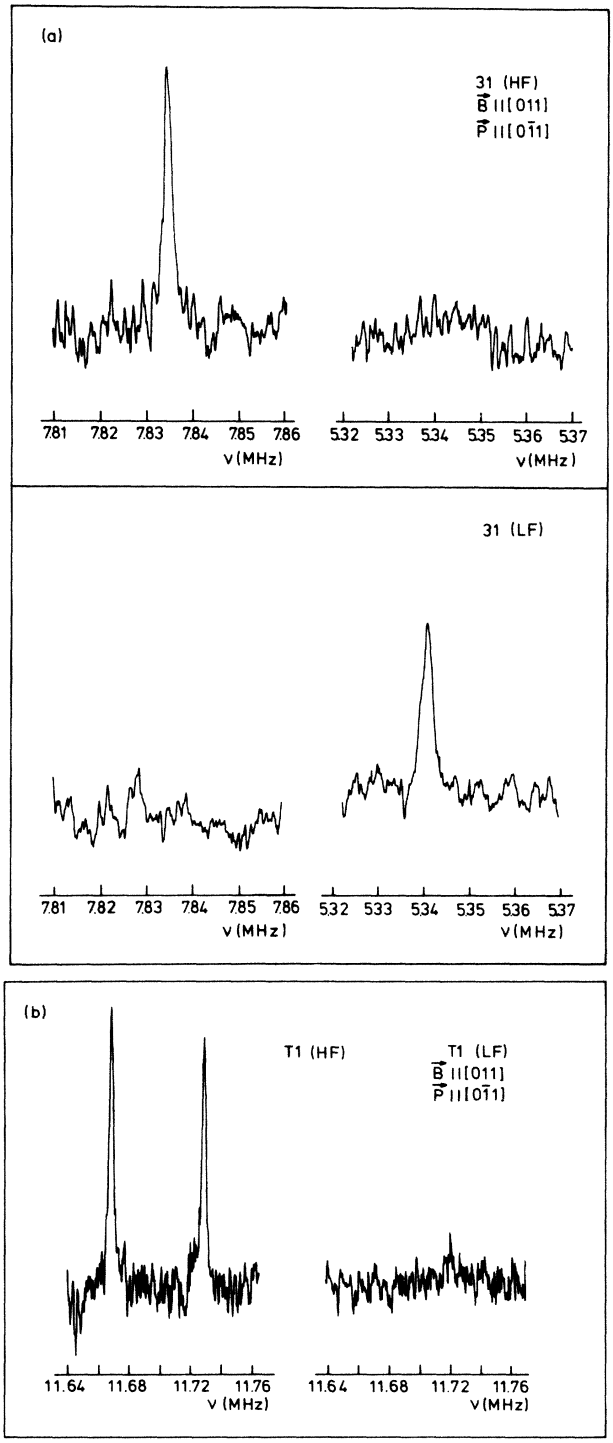


FIG. 4. Recorder traces of the Si:$Fe_i^0$ ENDOR spectrum at 1.5 K and $\nu_\mu = 22.5682$ GHz, $\mathbf{B}||[011]$ on the high-field (HF) and low-field (LF) resonance of Fig. 3. For the same Fe-$^{29}$Si orientation the ENDOR transitions above and below $\nu_z$ appear on different EPR components for tensor *31* (a). The shift of resonance frequency due to the difference in $B_{LF}$ and $B_{HF}$ is expected to be less than 10 kHz. Although the ENDOR lines above $\nu_z$ occur for both *31* (a) and *T1* (b) on the high-field resonance this does *not* lead to the same sign of $a'$ of these tensors. The resonances shown for *T1* do not coincide due to a small tilt of the magnetic field rotation plane with respect to the (0$\bar{1}$1) plane.

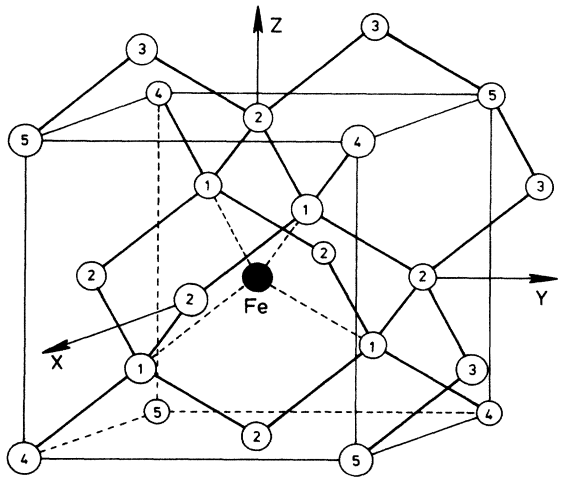


FIG. 5. The Fe interstitial (solid circle) surrounded by silicon atoms. This figure also shows the coordinate system on which the Cartesian hyperfine tensors and directions of eigenvectors of Table II are defined.

exclude any mistake we made a least-squares parameter fit to the observed resonances with a computer diagonalization of the Hamiltonian, Eq. (7), keeping the electronic $g$ value fixed at $g = 2.070$ and the nuclear $g$ value at $g_N = -1.1097$.[22] The parameters found were in agreement with those of Ref. 1.

Next we applied 4.4 MPa compressive stress along the [0$\bar{1}$1] direction, thereby causing the EPR line to split into its two fine-structure components and scanned the regions in which the resonances where found in the unstressed case, on both EPR lines separately. In the worst case ($M2$,$\mathbf{B}||[100]$) we observed a 2:1 intensity ratio of the ENDOR resonances above and below Zeeman frequency on the high-intensity EPR line; since this reversed on the low-intensity EPR line we may attribute this solely to the effect described in Sec. II B. Usually the effect was far more pronounced as can be seen in Fig. 4. The shift in resonance frequency was within 2 kHz consistent with the change in nuclear Zeeman frequency due to the difference in resonance field **B**; the effect of stress on ENDOR line positions is thus seen to be nearly negligible as expected. These results are summarized in Table II; the magnitude of the parameters is obtained from the unstressed data set and the overall signs of the tensors are as determined from the stressed ENDOR data, using an electronic $g$ value $g = +2.070$ and a nuclear $g$ value $g_N = -1.1097$. The sign of the $g$ value has been determined for several defects in silicon (including the interstitial $3d$ transition-metal $Cr^+$) and was always found to be positive;[23] the absolute signs of the hyperfine tensors are therefore probably as given in Table II. The tensors and directions of eigenvectors in this table are defined in the coordinate system of Fig. 5 and valid for the following.

(1) The atom on the [111] axis for shells *31*–*33*.

(2) One of the two atoms on the [001] axis for *T1*, since no unique assignment of the hyperfine tensor to one of these two atoms can be made.

TABLE II. Parameters, orientations, and signs of hyperfine tensors of $^{29}$Si neighbors of Si:Fe$_i^0$ (in kHz), as determined in this work. Tensors are given in Cartesian components and as principal values $A_i$ with corresponding principal directions $\hat{n}_i$. Experimental uncertainty is ±0.7 kHz.

| Shell | $\overleftrightarrow{A}$ | | | $i$ | $A_i$ | $\hat{n}_i$ |
|---|---|---|---|---|---|---|
| *31* | 157.6 | 1402.1 | 1402.1 | 1 | 2961.8 | (−0.577, −0.577, −0.577) |
| | 1402.1 | 157.6 | 1402.1 | 2 | −1244.5 | (+0.408, −0.816, +0.408) |
| | 1402.1 | 1402.1 | 157.6 | 3 | −1244.5 | (+0.707, +0.000, −0.707) |
| *32* | 776.5 | −196.3 | −196.3 | 1 | 383.9 | (−0.577, −0.577, −0.577) |
| | −196.3 | 776.5 | −196.3 | 2 | 972.8 | (+0.408, −0.816, +0.408) |
| | −196.3 | −196.3 | 776.5 | 3 | 972.8 | (+0.707, +0.000, −0.707) |
| *33* | 3244.7 | −156.7 | −156.7 | 1 | 2931.3 | (−0.577, −0.577, −0.577) |
| | −156.7 | 3244.7 | −156.7 | 2 | 3401.4 | (+0.408, −0.816, +0.408) |
| | −156.7 | −156.7 | 3244.7 | 3 | 3401.4 | (+0.707, +0.000, −0.707) |
| *T*1 | −3842.7 | −514.4 | 0.0 | 1 | −4357.1 | (−0.707, −0.707, +0.000) |
| | −514.4 | −3842.7 | 0.0 | 2 | −3328.3 | (−0.707, +0.707, +0.000) |
| | 0.0 | 0.0 | −6239.7 | 3 | −6239.7 | (+0.000, +0.000, +1.000) |
| *M*1 | −3729.0 | −361.4 | −435.7 | 1 | −3367.6 | (−0.707, +0.707, +0.000) |
| | −361.4 | −3729.0 | −435.7 | 2 | −3504.5 | (−0.512, −0.512, +0.689) |
| | −435.7 | −435.7 | −4152.4 | 3 | −4738.4 | (+0.487, +0.487, +0.725) |
| *M*2 | −398.5 | −99.0 | −74.8 | 1 | −299.6 | (−0.707, +0.707, +0.000) |
| | −99.0 | −398.5 | −74.8 | 2 | −292.7 | (+0.324, +0.324, −0.889) |
| | −74.8 | −74.8 | −347.3 | 3 | −552.1 | (−0.628, −0.628, −0.459) |

(3) One of the two atoms in the $(\bar{1}10)$ mirror plane, for shell *M*1 and *M*2 (as for *T*1).

Data for atoms in the shells, other than just specified, can be obtained by applying the appropriate symmetry transformations.

Typical widths of the resonances were 2–3 kHz full width at half maximum, allowing line positions to be determined with an accuracy of 0.7 kHz. The deviations of calculated ENDOR frequencies from experimental values were generally less than this value. The parameters of Table II are also given in terms of $a'$, $b'$, and $c'$ in Table III, allowing convenient comparison to the data of Greulich-Weber *et al.* in Table I.

## IV. DISCUSSION

The agreement between experimental and calculated values of $b'$ (point-dipole approximation) is clearly destroyed, due to the fact that tensor *31* is of opposite sign as chosen in Ref. 1. The assignment of experimental tensors to specific lattice sites is therefore no longer evident. All values of $a'$ of the *3*-class tensors have the same sign however, and are opposite to those of the other symmetry shells; this can be taken as clear evidence that $a'$ of the 3-class tensors ($a' > 0$) is not determined by spin transfer from the $e$ state, since an electron in a $3s$ orbital gives rise to a hyperfine interaction of $a_0 = -4749$ MHz.[24] In contrast, $a'$ of the other symmetry shells is negative, as ex-

TABLE III. Parameters, orientations, and signs of the $^{29}$Si hyperfine interaction of the Si:Fe$_i^0$ system in terms of $a'$, $b'$, and $c'$ (in kHz), this work. Experimental uncertainty is ±0.7 kHz.

| Tensor | $a'$ | $b'$ | $c'$ | $Z_{hf}$ | Shell assignment 1 | 2 | 3 |
|---|---|---|---|---|---|---|---|
| *31* | 157.6 | 1402.1 | 0 | [111] | 1 | 4 or 5 | 4 or 5 |
| *32* | 776.5 | −196.3 | 0 | [111] | 4 or 5 | 1 | 5 or 4 |
| *33* | 3244.7 | −156.7 | 0 | [111] | 5 or 4 | 5 or 4 | 1 |
| *T*1 | −4641.7 | −799.0 | −514.4 | [100] | 2 | 2 | 2 |
| *M*1 | −3870.2 | −434.1 | +68.5 | $<$[111]$=11.2°$ | 3 | 3 | 3 |
| *M*2 | −381.4 | −85.3 | −3.5 | $<$[111]$=7.9°$ | 6 | 6 | 6 |

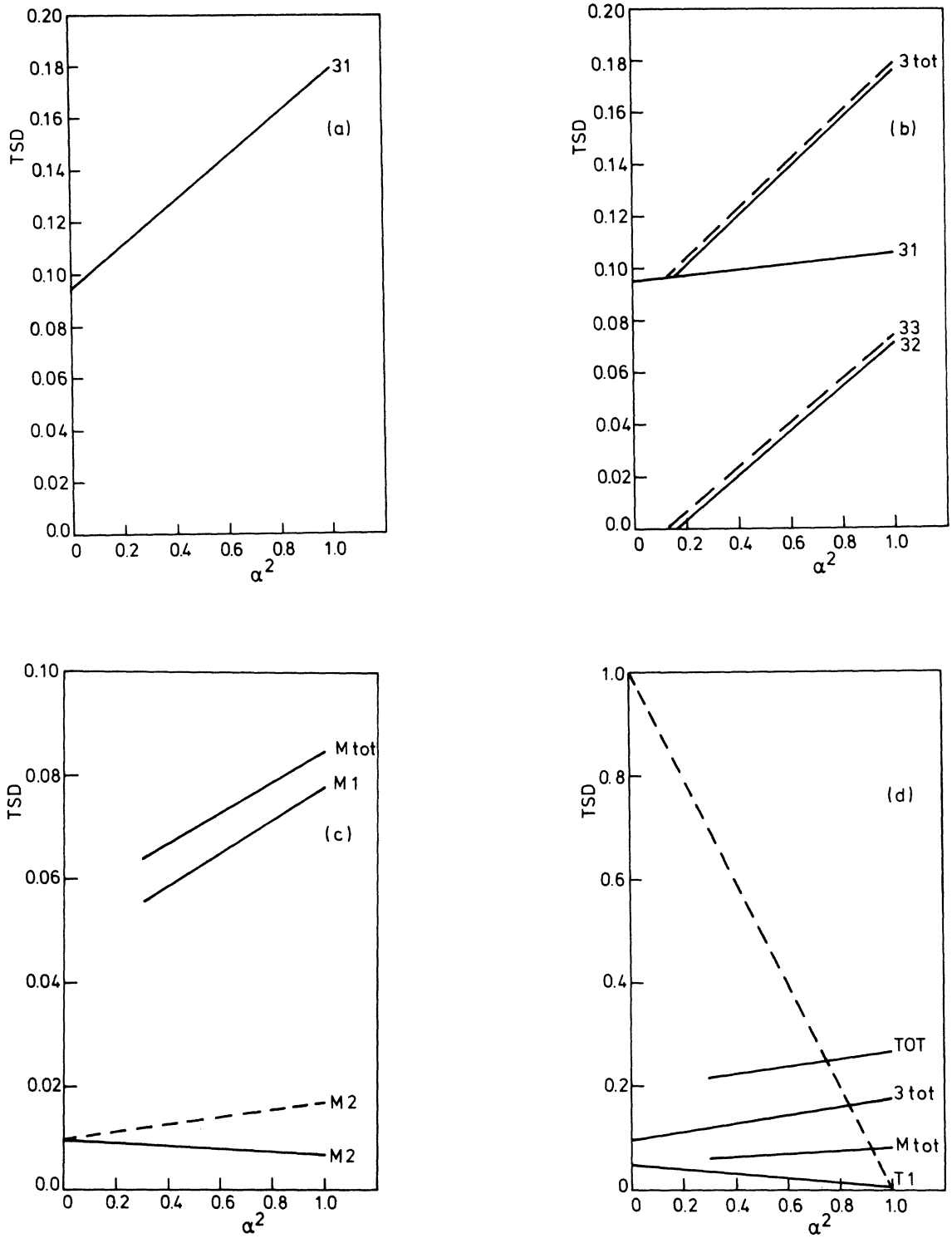


FIG. 6. Transferred spin densities (TSD's) to the lattice versus spin localization $\alpha^2$ on the Fe atom, as obtained from the hyperfine interaction tensors in the assignments of Table III. (a) *3*-class shells, assignment 1. Tensor *32* and *33* do not contribute any TSD in this assignment (see the text). (b) *3*-class shells. In assignment 2 only tensors *31* and *32* contribute TSD (solid line); in assignment 3 tensor *32* does not contribute (dashed line). The TSD obtained from *31* is equal in both these assignments. (c) *m*-class shells. In the case of *M*1 only one assignment (within the $\bar{3}\,\bar{1}\,\bar{1}$ shell) yielded real coefficients for the symmetry orbitals ($\alpha^2 > 0.3$). In the case of *M*2 both assignments within the 331 shell yielded real coefficients, indicated by the solid and the dashed line. The former is used in calculating $M_{\text{tot}}$ and the total TSD. (d) Total TSD of all measured shells in assignment 1. The dashed line gives the connection between transferred and Fe-localized spin density.

pected, since for them spin transfer to the silicon $3s$ orbitals is symmetry allowed. This conclusion is independent of the sign of the $g$ value, since $a'$ and $a_0$ will reverse sign simultaneously if the $g$ value would appear to be negative. This observation therefore confirms the $e$ symmetry of the ground state.

In contrast to the case of $Ti^+$ it is possible to determine the wave-function coefficients $\beta_i^2$, $\gamma_i^2$, $\delta_i^2$, and $\epsilon_i^2$ uniquely from the experimental hyperfine interaction parameters and to extract exact transferred spin densities (TSD's), using the values for $|s_1(0)|^2$ and $\langle r^{-3}\rangle_p$,[24] once an assignment of tensors to specific lattice sites has been made. We will analyze the $Fe_i^0$ data for three possible assignments of these tensors, summarized in Table III (notation as in Ref. 2). In all these assignments the total TSD is about the same, but in assignment 1 the distribution of the spin density over the lattice is considerably different from that obtained in assignments 2 and 3. In the former case the spin density is mainly concentrated on the first shell and no spin density can be obtained from $\mathcal{3}2$ and $\mathcal{3}3$ [Fig. 6(a)], since $b'$ after correction for $b_{dd}$ is of the wrong sign with respect to Eq. (2). Assignments 2 and 3 both yield a spin density on the first nearest-neighbor shell that is of comparable magnitude to that on the next $\mathcal{3}$-class shell (it is even smaller), which is somewhat contrary to our intuitive expectations [Fig. 6(b)]. No TSD values can be obtained for $M1$ for values of $\alpha^2 < 0.3$ without allowing imaginary coefficients in the expressions for the symmetry orbitals [Fig. 6(c)]. Since this corresponds to a spin delocalization of over 70%, whereas the reduction in central nucleus hyperfine parameter $A$ amounts to 43%, such a situation is not likely to occur.

The total spin delocalization and the contributions from the three classes of neighboring sites is shown in Fig. 6(d). The dashed line in this figure represents the normalization condition

$$\alpha^2+\sum_i(\beta_i^2+\gamma_i^2+\delta_i^2+\epsilon_i^2)=1$$

in which overlap integrals have been omitted. Inclusion of these terms requires a more detailed knowledge of the spatial extent of the atomic orbitals, while their influence on the estimate of the total TSD is only marginal as evidenced by Fig. 6(d). In assignment 1 we therefore obtain a spin localization of 25% on the six shells measured, which is only slightly less in assignments 2 and 3. This estimate complies well with the observed reduction in central nucleus hyperfine interaction parameter $A$ and is in remarkable good agreement with the Green's-function calculations by Katayama-Yoshida and Zunger who predict a 29% spin delocalization. In contrast to the $Ti_i^+$ system the bulk of the transferred spin is not on the second-neighbor shell, but rather on the first shell. Differently stated: the $t_2$ state seems to be mainly hybridized with the second-neighbor shell orbitals, while the $e$ state is mainly hybridized with orbitals on the first shell. It would be interesting to see whether this could be experimentally confirmed in another transition-metal system in silicon or be produced in theoretical calculations.

The fact that tensors $\mathcal{3}2$ and $\mathcal{3}3$ do not yield a spin density in assignment 1 means that the spin density drops very fast with distance from the Fe nucleus; on the iron nucleus itself we find approximately 75% of the spin density, ~16% on the first nearest-neighbor shell, on the third shell ~8%, and next to nothing on the other shells (which makes the iron system a good candidate for a cluster calculation). There remains a part of $b'$ unexplained for tensors $\mathcal{3}2$ and $\mathcal{3}3$ in this assignment; they still yield some −35 and −75 kHz anisotropic hyperfine interaction after subtraction of the distant dipole-dipole interaction with the central nucleus (−125 kHz for 75% Fe localization). As it is of the same sign as $b_{dd}$, it must be due to a spin density in the $\sigma$ orbitals (forbidden) or due to multicenter contributions. The latter is probably the case as one can see by calculating, for instance, the contribution to $b'$ on the 222 lattice site due to the spin density on the 111 position (~4%) in the point-dipole approximation, yielding an extra −50 kHz. Similarly we can calculate the contribution to the off-diagonal element of $T1$ (−514 kHz) for atom 002 in the second shell from the spin density on atoms 111 and $\bar{1}\,\bar{1}1$ of the first shell in assignment 1, which amounts to ~−100 kHz in the point-dipole approximation. The contribution from the matrix element

$$\left\langle d_{3z^2-r^2}\left|\frac{xy}{r^3}\right|\sigma_1\right\rangle$$

is zero for symmetry reasons and contributions from the other shells can be neglected with respect to that from the first shell. Clearly these multicenter contributions cannot explain the observed value of $c'$ ($T1$) and we are therefore led to conclude that it is probably caused by transfer from the spin-polarized $t_2$ state, confirming the Green's-function results from Katayama-Yoshida and Zunger. The occurrence of positive values of $a'$ for the $\mathcal{3}$-class shells is not in contrast to this, although the data do not exclude the possibility that the aforementioned effects originate in part (or completely) from spin polarization of orbitals transforming according to other irreducible representations of the $\bar{4}3m$ symmetry group than $t_2$.

## V. CONCLUSIONS

The contradiction between the observed reduction in central nucleus hyperfine parameter, indicating a relatively delocalized spin density, and the ENDOR data of Greulich-Weber *et al.*, leading in their view to a highly localized spin density, can be eliminated by a reinterpretation of their data. The experimental determination of the signs of the hyperfine interaction tensors, as presented here, strongly supports this reinterpretation and leads to a fairly delocalized spin density (25%), in good agreement with the spin-polarized self-consistent Green's-function calculations by Katayama-Yoshida and Zunger.

## ACKNOWLEDGMENT

This work received financial support from the Netherlands Foundation for Fundamental Research on Matter (FOM).

*Permanent address: Institute of Physics, Polish Academy of Sciences, Warsaw, Poland.

[1]S. Greulich-Weber, J. R. Niklas, E. R. Weber, and J. M. Spaeth, Phys. Rev. B **30**, 6292 (1984).

[2]D. A. van Wezep, R. van Kemp, E. G. Sieverts, and C. A. J. Ammerlaan, Phys. Rev. B **32**, 7129 (1985).

[3]J. G. de Wit, E. G. Sieverts, and C. A. J. Ammerlaan, Phys. Rev. B **14**, 3494 (1976).

[4]E. G. Sieverts, S. H. Muller, and C. A. J. Ammerlaan, Phys. Rev. B **18**, 6834 (1978).

[5]G. W. Ludwig, Phys. Rev. **137**, A1520 (1965).

[6]J. R. Niklas and J. M. Spaeth, Solid State Commun. **46**, 121 (1983).

[7]S. Greulich-Weber, J. R. Niklas, and J. M. Spaeth, J. Phys. C **17**, L911 (1984).

[8]G. Feher, Phys. Rev. **114**, 1219 (1959).

[9]E. B. Hale and R. L. Mieher, Phys. Rev. **184**, 739 (1969).

[10]H. Katayama-Yoshida and A. Zunger, Phys. Rev. Lett. **53**, 1256 (1984); Phys. Rev. B **31**, 7877 (1985).

[11]H. Katayama-Yoshida and A. Zunger, Phys. Rev. B **31**, 8317 (1985).

[12]F. Beeler, O. K. Andersen, and M. Scheffler, Phys. Rev. Lett. **55**, 1498 (1985).

[13]G. W. Ludwig and H. H. Woodbury, in *Solid State Physics*, edited by F. Seitz and D. Turnbull (Academic, New York, 1962), Vol. 13, p. 223 ff.

[14]R. E. Watson and A. J. Freeman, in *Hyperfine Interactions*, edited by A. J. Freeman and R. B. Frankel (Academic, New York, 1967), p. 53 ff.

[15]D. A. van Wezep and C. A. J. Ammerlaan, J. Electron. Mater. **14a**, 863 (1985).

[16]E. G. Sieverts, S. H. Muller, C. A. J. Ammerlaan, and E. R. Weber, Solid State Commun. **47**, 631 (1983).

[17]J. Owen and J. H. M. Thornley, Rep. Prog. Phys. **29**, 675 (1966).

[18]G. D. Watkins and J. W. Corbett, Phys. Rev. **134**, A1359 (1964).

[19]D. A. van Wezep and C. A. J. Ammerlaan (unpublished).

[20]R. van Kemp, E. G. Sieverts, and C. A. J. Ammerlaan (unpublished).

[21]M. Berke, E. Weber, H. Alexander, H. Luft, and B. Elschner, Solid State Commun. **20**, 881 (1976).

[22]M. Sprenger, S. H. Muller, and C. A. J. Ammerlaan, Physica **116B**, 224 (1983). The value of $g_N$ mentioned here has been slightly corrected [M. Sprenger (private communication)].

[23]F. V. Strnisa and J. W. Corbett, Cryst. Lattice Defects **5**, 261 (1974).

[24]J. R. Morton and K. F. Preston, J. Magn. Reson. **30**, 577 (1978).